ELSEVIER

Journal of Nuclear Materials 265 (1999) 1–11

journal of nuclear materials

On the effects of heat treatment and surface orientation on corrosion and hydrogen ingress of Zr–2.5Nb pressure tube material

Y.-P. Lin *, J. DeLuca

Ontario Hydro Technologies, 800 Kipling Ave, Toronto, Ont., Canada M8Z 5S4

Received 17 March 1998; accepted 19 October 1998

Abstract

The influences of surface orientation and heat treatment on the corrosion and hydrogen pickup of Zr–2.5Nb pressure tube material have been investigated. Following a prefilm treatment in 673 K steam and exposure to lithiated water (pH 10.5) at 583 K, the increase in oxide thickness and the pickup of hydrogen during a 120-day exposure at 583 K were monitored. In addition to being sensitive to the heat treatment given, the corrosion and hydrogen pickup were affected by the alignment of β-Zr with respect to the oxide surface. An enhanced oxide growth is associated with the initially undecomposed β-Zr aligned primarily perpendicular to the oxide surface. A minor effect on oxide growth is attributed to changes in the dislocation substructure due to heat treatment. A reduced hydrogen pickup is associated with β-Zr initially in the partially or fully decomposed states and aligned primarily perpendicular to the oxide surface.

1. Introduction

The Zr–2.5Nb alloy is used as the pressure tube material in CANDU reactors. The pr*essure tubes are manufactured by extrusion and cold drawing and the resultant microstructure and texture are anisotropic [1,2]. Grains of the primary, hexagonal-close-packed α-Zr phase (<1% Nb) are elongated along the axial direction, and have a preferred alignment of [1 $\bar{1}$ 0 0] along the tube axis and [0 0 0 1] along the tangential direction. The α-Zr grains are typically 0.3–0.5 μm thick in the radial direction and are often surrounded by a thin layer of body-centred-cubic (bcc) β-Zr (∼20% Nb). The detailed microstructure within the β-Zr is sensitive to subsequent heat treatments. Since β-Zr is a metastable phase below the monotectoid temperature, it will eventually transform to the equilibrium β-Nb (>85% Nb, also bcc). Depending on the exposure conditions, the transformation may involve the formation of an intermediate ω-phase with an associated Nb enrichment in the surrounding β-Zr [3].

A corrosion oxide film is formed on the tube surface during the last stage of tube manufacture and continues to grow during subsequent service exposures. The corrosion process and the concomitant pickup of a small amount of corrosion-released hydrogen are both of interest to the performance of the pressure tubes. Examinations of pressure tubes removed from reactors have shown that there are variations between tubes with respect to their corrosion and hydrogen pickup behaviour [4]. A material related variability in out-reactor autoclave experiments is also observed between different pressure tube coupons subjected to identical exposures [5].

The aim of the present work is to understand better the variations in corrosion and hydrogen pickup due to changes in the pressure tube microstructure. In the present experiment, coupons with different surface orientations have been prepared from a Zr–2.5Nb pressure tube and different heat treatments were applied prior to the corrosion exposure. As the coupons were prepared from the same pressure tube section, the effect due to

* Corresponding author.

0022-3115/99/$ – see front matter
PII: S0022-3115(98)00655-2

variations in composition or impurity content is minimal. As the morphology of the β-Zr is anisotropic, the use of different surface orientations allowed the effect due to β-Zr to be assessed.

2. Experimental

As-received (AR) material from a pressure tube (H365M, see Table 1 for composition) in the as-cold-drawn condition was used in the present work. Sets of broad but thin coupons (≈1 mm in thickness) were prepared in which the largest exposed face corresponded to the radial-normal (RN), the tangential-normal (TN) or the axial-normal (AN) surfaces of the pressure tube, Fig. 1. The coupon dimensions were typically $25 \times 10 \times 1$, $30 \times 4 \times 1$ and $30 \times 4 \times 1$ mm, respectively. In addition, two sets of samples were prepared whose surfaces were slightly tilted (less than 15°) away from the RN orientation (RN-a and RN-b) and another set was prepared whose surface orientation was at 30° from the AN surface tilted about the tangential direction (AN-a). For the present purpose, RN samples will refer to the RN, RN-a and RN-b sets and non-RN samples will refer to the TN, AN and AN-a sets.

The choice of broad but thin sample dimensions was to ensure that the hydrogen pickup arose primarily from the oxide formed on the surface of interest. The coupons were used either in the AR condition or in heat-treated conditions. One group of coupons was heat treated for 100 h at 673 K and another group was heat treated for 6 h at 773 K. Prior to exposures to form oxide, all coupons were chemically polished using a 15% HNO_3/30% H_2SO_4/10% HF/H_2O mixture. The coupons were subjected to three oxide-forming exposures. The first exposure, the prefilm exposure, was in steam at 673 K. Coupons from all combinations of surface orientations and material conditions were prefilmed for 24 h. A smaller set of samples was prefilmed for 350 h. All prefilmed samples were exposed for 56 days in lithiated water (pH 10.5) at 583 K. The oxide thickness after this exposure was measured using Fourier transform infrared spectroscopy (FTIR). A small piece of material was cut from each coupon and used for the analysis of hydrogen content using differential scanning calorimetry (DSC). The final exposure was for 120 days in lithiated water (pH 10.5) at 583 K, after which the oxide thickness and hydrogen content were re-measured.

For microstructural investigations, electropolished thin foils were prepared using a 10% perchloric acid in methanol mixture at 233 K and examined in a JEOL 2010 analytical transmission electron microscope (TEM) equipped with energy dispersive spectroscopy (EDS) capability. Plan-view foils of oxides for TEM examinations were prepared by chemical removal of the underlying metal. For thin oxides (<0.2 μm) the foils were examined without additional preparation. For thicker oxide films, ion milling was applied to achieve electron transparency. The oxide undersides of selected samples were examined in a field emission scanning electron microscope (SEM) following the chemical removal of the underlying metal.

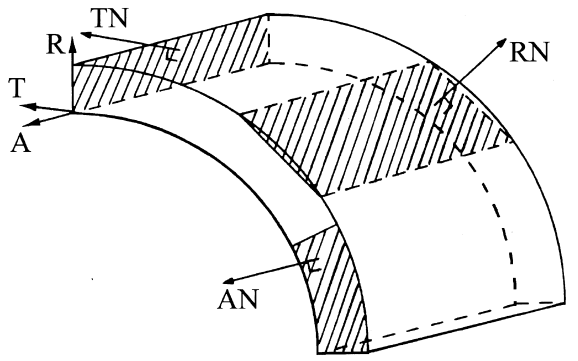

Fig. 1. Schematic diagram showing the orientation of the Radial-Normal (RN), Axial-Normal (AN) and Tangential-Normal (TN) sections relative to the principal Radial (R), Axial (A) and Tangential (T) directions of a pressure tube.

3. Results and discussion

The present set of surface orientations and prior heat treatments introduced variations in several microstructural parameters. The different surface orientations meant that the surface crystal orientations, i.e. textures, of α-Zr and the morphologies of β-Zr were different. The heat treatments given prior to corrosion exposures affected the decomposition of the metastable β-Zr as well as the recovery of lattice defects and residual stresses introduced by cold drawing. The composition of the α-Zr may also be affected by the heat treatments. It is recognised that these changes can continue during oxide growth exposures, particularly during the higher temperature pre-film exposure and for the AR material.

The combined thickness of the oxide formed during the prefilmed treatment and the 56-day 583 K exposure exhibited considerable variation as shown in Table 2.

Table 1
Composition of pressure tube H365M based on ingot analysis

Nb (wt%)	O (ppm)	C (ppm)	Fe (ppm)	N (ppm)	Si (ppm)	Zr
2.5	1130	145	430	34	<60	balance

Table 2
Oxide thickness after prefilm in steam at 673 K and exposure to lithiated water at 583 K for 56 days (in μm)

Material condition	Prefilm time (h)	Surface orientation					
		RN	RN-a	RN-b	TN	AN	AN-a
AR	24	1.76	1.76	1.84	2.92	3.03	2.87
						3.01	
AR	350	2.67					
AR + 100 h 673 K	24	1.80	1.66	1.78	1.75	1.66	1.79
					1.69	1.63	
AR + 100 h 673 K	350	1.84			1.81	1.74	1.90
					1.67	2.10	
AR + 6 h 773 K	24	1.49	1.45	1.52	1.48	1.45	1.67
					1.52	1.66	
AR + 6 h 773 K	350	1.42					

For the subsequent 120-day 583 K lithiated water exposure, an incremental change in oxide thickness of between about 0.7 and 0.8 μm was measured for most coupons, in Table 3, the exception being the RN coupon initially in the AR condition, which exhibited an increase of 1.1 μm. The corresponding hydrogen pickup during this 120-day exposure is given in Tables 4 and 5.

3.1. Variations in oxide growth

The results in Table 2 show that the differences in the oxidation behaviour between the three surface orientations occurred in materials in the AR condition but not in either of the heat-treated conditions. The RN and non-RN surface orientations have quite dissimilar α-Zr textures. Since the heat treatment conditions used were not expected to have produced significant changes to the α-Zr texture, it follows that the variation in oxide thickness between the three surface orientations of the AR material was not related to the texture of α-Zr.

A significant difference between the RN surface orientation and the non-RN surface orientations was the morphology of the β-Zr phase. The non-RN surfaces were microstructurally similar in that more β-Zr filaments were aligned perpendicular to the surface compared with the RN surfaces. In Table 2, the enhanced oxide growth on the non-RN surfaces compared with the RN surface in the AR condition can be attributed to this difference in β-Zr alignment. The cause for enhanced oxide growth was provided by SEM examination of oxide undersides, Fig. 2. The samples examined were the AN oxides after the prefilm treatment (24 h at 673 K) and 56 days exposure at 583 K. The SEM samples were prepared such that the viewing direction was along the tangential direction of the pressure tube as depicted in Fig. 2(a). In this specimen geometry, the β-Zr filaments were oriented primarily perpendicular to the oxide surface. For the material initially in the AR condition, the oxide underside contained ridges that may be correlated with β-Zr filaments, Fig. 2(b). For materials heat-treated prior to corrosion exposures, such ridges were absent, Figs. 2(c) and 2(d).

Additional support for a local increased oxidation rate associated with β-Zr was obtained from TEM examinations. As an example, a plan-view TEM image of a thin (0.2 μm thick) oxide formed in steam at 673 K on a RN surface initially in the AR condition is shown in Fig. 3. Bands of thicker oxide (dark appearance) can be readily identified with the morphology of β-Zr. Imaging of the foil at different tilts showed that these bands

Table 3
Increase in oxide thickness due to 120-day exposure to lithiated water at 583 K (in μm)

Material condition	Prefilm time (h)	Surface orientation					
		RN	RN-a	RN-b	TN	AN	AN-a
AR	24	1.09	0.86	0.81	0.78	0.73	0.67
						0.70	
AR	350	0.86					
AR + 100 h 673 K	24	0.68	0.84	0.67	0.98	0.80	0.74
					0.75	0.87	
AR + 100 h 673 K	350	0.75			0.71	0.72	0.81
					0.79	0.99	
AR + 6 h 773 K	24	0.72	0.70	0.72	0.69	0.77	0.80
					0.76	0.68	
AR + 6 h 773 K	350	0.78					

Table 4
Hydrogen (hydrogen equivalent) pickup during 120-day exposure to lithiated water at 583 K (in μg/cm^2)

Material condition	Prefilm time (h)	Surface orientation					
		RN			Non-RN		
		RN	RN-a	RN-b	TN	AN	AN-a
AR	24	1.99	1.45	1.48	2.00	1.24	1.23
						1.26	
AR	350	1.25					
AR + 100 h 673 K	24	1.46	1.11	1.29	0.88	0.53	0.62
					0.63	0.53	
AR + 100 h 673 K	350	1.38			1.35	0.48	0.75
					1.01	1.44	
AR + 6 h 773 K	24	1.20	1.05	0.91	0.43	0.20	0.43
					0.49	0.53	
AR + 6 h 773 K	350	0.90					

corresponded to 'tongues' or protrusions into the metal (that had been removed). The association of ridges or protrusions with β-Zr is consistent with a lower corrosion resistance reported for Zr–20Nb, a composition similar to β-Zr, compared with Zr–1Nb (α-Zr) [6], and with previous observations on oxides of Zr–2.5Nb material [7–10]. Present SEM and TEM observations indicate that enhanced oxide growth resulted from the lateral growth and coalescence of protrusions or ridges formed on α-Zr adjacent to β-Zr. Such an enhanced growth is most effective for β-Zr initially in the undecomposed state and aligned perpendicular to the oxide surface, i.e. non-RN surfaces. For the RN surface, such a growth mechanism is not effective, since the β-Zr filaments are aligned primarily parallel with the oxide surface, and the spacing is greater between the locations where β-Zr intersected the oxide surface.

It should be pointed out that the pressure tube microstructure is not always uniform. There are regions in pressure tubes where the local β-morphology (and α-Zr texture) deviates from the idealised description given above. The sensitivity of oxidation behaviour to the morphology of β-Zr suggests that microstructural inhomogeneity may be a possible factor contributing towards non-uniform corrosion, such as thick oxide patches, which is know to occur in pressure tubes under operating conditions.

3.2. Effect of heat treatment on β-Zr

As the enhanced growth was associated with β-Zr, it follows that the elimination of the enhanced growth due to prior heat treatments was related to changes in β-Zr. A similar effect has been reported [6] in which the corrosion rate for the β-Zr alloy (Zr–20Nb) was reduced to a level similar to α-Zr alloy (Zr–1Nb) due to decomposition during exposure. In the present work, changes to β-Zr brought about by heat treatment and during exposure were examined using TEM. The observed microstructural changes are consistent with

Table 5
Percentage hydrogen (hydrogen equivalent) pickup during 120-day exposure to lithiated water at 583 K (in %)

Material condition	Prefilm time (h)	Surface orientation					
		RN			Non-RN		
		RN	RN-a	RN-b	TN	AN	AN-a
AR	24	4.78	5.10	4.40	7.01	4.64	5.44
						4.92	
AR	350	3.91					
AR + 100 h 673 K	24	4.99	3.75	5.17	2.46	1.82	2.22
					2.36	1.67	
AR + 100 h 673 K	350	4.85			5.20	1.82	2.71
					3.51	4.00	
AR + 6 h 773 K	24	4.98	4.05	3.50	1.96	0.71	1.46
					1.75	2.11	
AR + 6 h 773 K	350	3.38					

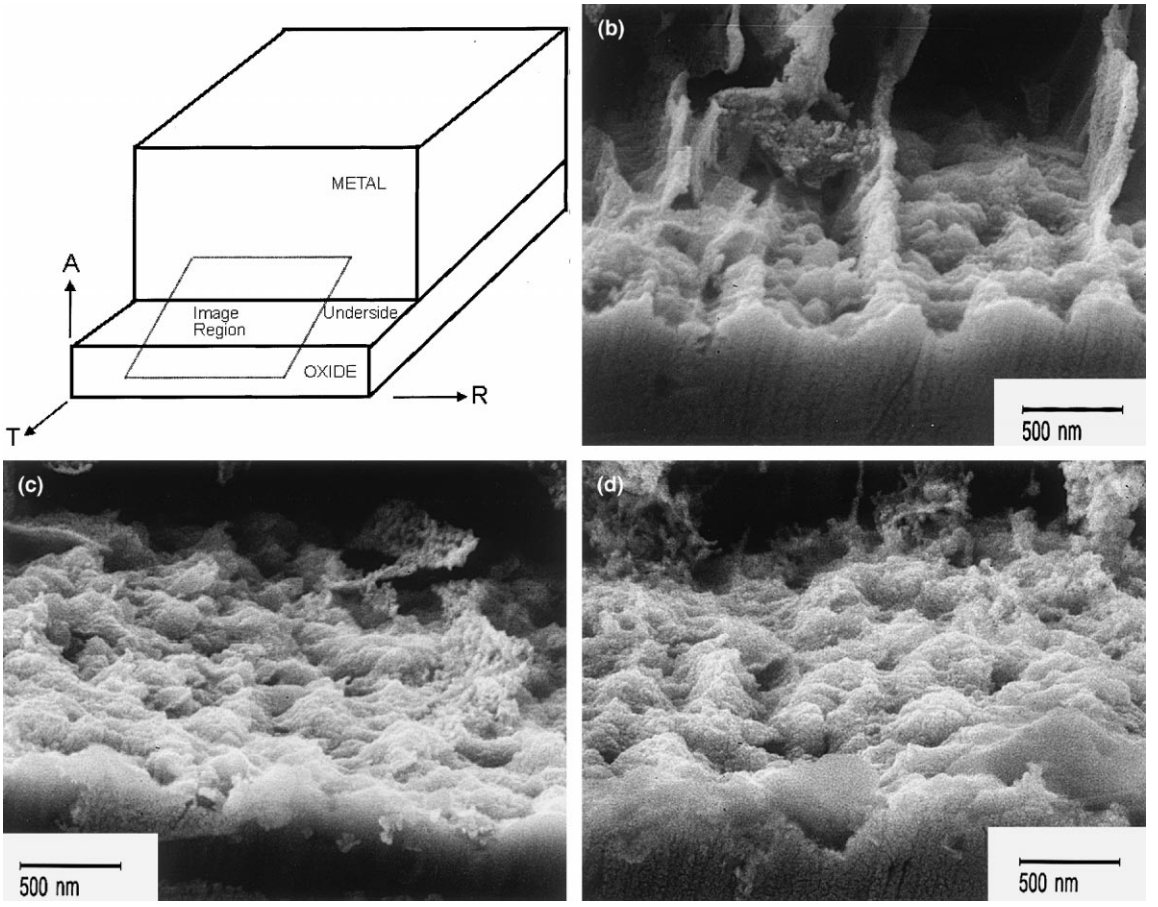

Fig. 2. SEM imaging of oxide undersides. (a) Sample and imaging geometry. R, T, and A refer to the Radial, Tangential and Axial directions of the pressure tube respectfully. (b) Underside of oxide on AN surface initially in the AR condition; oxide was formed during exposure for 24 h at 673 K followed by 56 days aqueous exposure at 583 K. (c) as (b) but for the 673 K treated material. (d) as (b) but for the 773 K treated material.

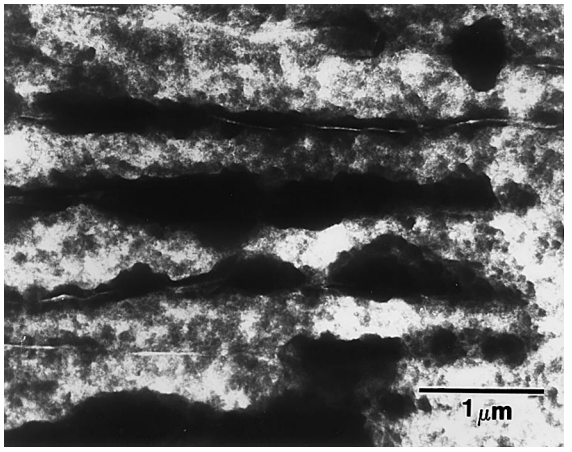

Fig. 3. Plan-view TEM image of a 0.2 μm thick oxide formed in 673 K steam showing protrusions adjacent to β-Zr. No thinning was applied to the oxide film imaged.

previous observations on decomposition of β-Zr [3,4,11,12]. For the AR material, the undecomposed state of the β-Zr was indicated by the continuous morphology and uniform contrast, as illustrated in Fig. 4(a). After a 24 h, 673 K prefilm treatment and subsequent exposure for 56 days at 583 K, the β-Zr regions had partially decomposed to a state consisting of Nb-depleted ω particles surrounded by channels of β that were enriched in Nb.

A similar ω + Nb-enriched β morphology was observed in materials heat treated for 100 h at 673 K, Fig. 4(b). Corrosion exposures for 24 h at 673 K followed by 56 days at 583 K did not produce significant differences in the ω + Nb-enriched β microstructure. It was evident that despite having undergone a partial decomposition to the ω + Nb-enriched β configuration, the overall β regions were still continuous in the 673 K treated material, similar to the β-Zr in the AR condition. The absence of an

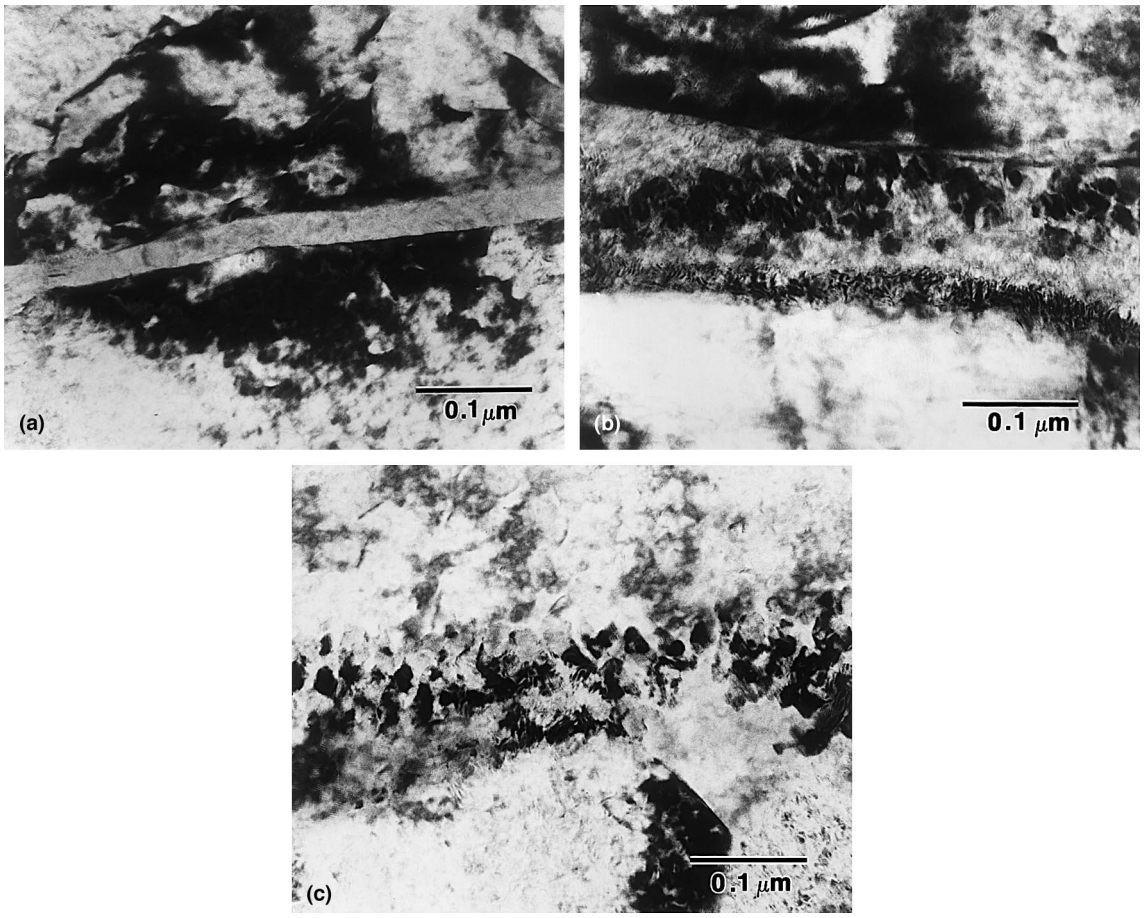

Fig. 4. TEM micrographs of β-Zr/β-Nb morphology (a) in the AR condition showing general uniform contrast within β-Zr band, (b) after 100 h heat treatment at 673 K showing contrast within β-Zr band due to ω-phase and (c) after 6 h at 773 K showing discrete morphology of β-Nb.

enhanced oxide growth in the 673 K treated non-RN samples, which contained β filaments perpendicular to the oxide surface, indicated that the morphology of β phase was an insufficient condition for promoting an enhanced oxide growth; the microstructure within the β filaments was important. The conclusion that both an undecomposed state and an appropriate morphology of the β-Zr are needed for an enhanced oxide growth is consistent with the observation that the amount of metastable β-Zr is not the critical factor in determining the corrosion behaviour of alloys of different Nb concentrations provided a continuous network of β-Zr was present [13].

For materials heat-treated for 6 h at 773 K, the original β-Zr had transformed into the equilibrium, Nb-rich β-Nb with an associated change in morphology. The β-Nb was less continuous and was present as a two-dimensional array of discrete particles, Fig. 4(c), corresponding to the β-Zr originally present. The absence of an enhanced oxide growth in the 773 K treated non-RN samples may be associated with both compositional (from β-Zr to β-Nb) and morphological changes.

With respect to providing an enhanced growth mechanism, the present results show that changes within the original β-Zr regions introduced by heat treatment are more significant than the presence of β-Zr aligned perpendicular to the oxide surface.

3.3. Effect due to changes in α-Zr

Table 2 showed that the heat treatment applied prior to the corrosion exposure affected the corrosion behaviour. In the previous section, a major component of the heat treatment effect was discussed in terms of the heat treatment induced changes in β-Zr. However, there are evidences in Table 2 that indicated that a heat treatment induced effect, though minor, was present due to changes in α-Zr, the primary phase of the alloy. One indication comes from the comparison of the 24 and 350 h prefilmed RN samples. As the prefilm temperature (673

K) was higher than the lithiated water exposure (583 K), the majority of the oxide was formed during the prefilm stage. In Table 2, the presence of a difference (24 versus 350 h) for the AR-RN material and the absence of significant differences for the heat-treated RN materials indicate a reduction in the oxide growth kinetics for the heat-treated materials under the prefilm condition. Since the corrosion behaviour of RN sections is not strongly affected by β-Zr, this reduction would appear to be related to changes in α-Zr. A more positive indication of an α-Zr effect is provided by noting that the oxides developed on both RN and non-RN orientations of the 773 K heat-treated material were consistently thinner than those on the 673 K treated material. In this case, any effect due to decomposition of β-Zr was minimal as all surface orientations behaved similarly.

To account for the minor improvement in corrosion resistance discussed above, two factors have been considered, namely changes in the Nb content in the α-Zr and recovery of the cold-worked dislocations. The extent of possible changes in Nb composition due to heat treatments and exposures was assessed by obtaining EDS measurements from α-Zr in three conditions. The three conditions were: (i) AR material without additional exposure, (ii) AR material with a heat treatment of 100 h at 673 K followed by exposures to 350 h at 673 K plus 56 days at 583 K and (iii) AR material with a heat treatment of 6 h at 773 K and exposures to 24 h at 673 K plus 56 days at 583 K. The expected detection limit for Nb in Zr is about 0.1 wt% for the experimental conditions used. Two spectra from α-Zr in each of the three conditions are shown in Fig. 5. The near identical spectra in Fig. 5 show that the Nb concentration in the α-Zr in the AR condition after extrusion and cold-drawing was not substantially different than that after heat treatments or post-heat treatment corrosion exposures. The Nb concentrations were estimated to be around 0.6–0.7 wt%, consistent with previous EDS measurements on Zr–2.5Nb pressure tube material [11,12] and with the maximum solubility for Nb in α-Zr reported in experimentally determined [14] and calculated [15] Zr–Nb phase diagrams. The reduction in oxide growth due to heat treatments is thus not attributable to changes in the Nb concentration in α-Zr, under the present experimental conditions. Under different conditions, a reduction in Nb content leading to an improvement in the corrosion response has been reported, due to the precipitation of β-Nb from the non-equilibrium martensitic α′-Zr in quenched Zr–2.5Nb [4,7,13,16–24] or from α-Zr in irradiated Zr-2.5Nb pressure tube material [25].

The second factor considered is the recovery of lattice defects. These changes were investigated qualitatively using the TEM. A high density of ⟨a⟩-component and some ⟨c⟩-component dislocations due to cold drawing were readily observed in the AR material, Fig. 6(a) and

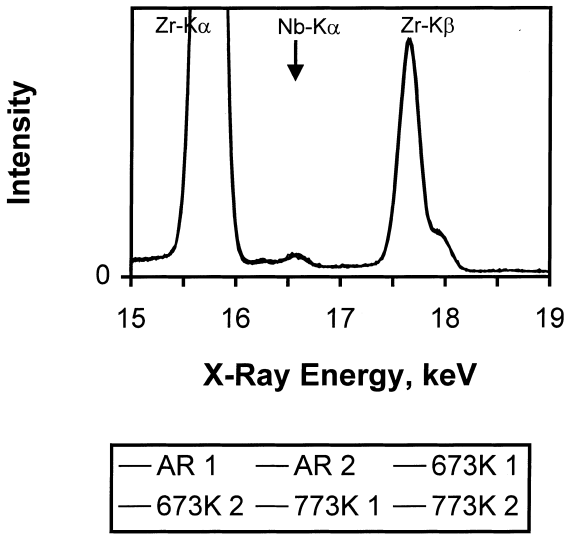

Fig. 5. Zr–K and Nb–K region of EDS spectra showing Nb content in α-Zr for materials in (i) the AR condition, (ii) AR plus exposures to 450 h at 673 K followed by 56 days at 583 K (marked as 673 K) and (iii) AR plus exposures to 6 h at 773 K followed by 24 h at 673 K and 56 days at 583 K (marked as 773 K). Two spectra per condition are shown. All spectra are scaled to the same Zr–K_α intensity and are superimposed on each other to demonstrate the similarity.

(b). In Fig. 6(a), the high density of dislocations is evident from the close spacing between dislocations. In the material subjected to a heat treatment of 100 h at 673 K, some recovery is expected, although many ⟨a⟩-component dislocations remained readily visible, as were ⟨c⟩-component dislocations. In the material heat treated for 6 h at 773 K, a more substantial recovery was evident, resulting in a general absence of ⟨c⟩-component dislocations and fewer ⟨a⟩-component dislocations, Fig. 6(c). In Fig. 6(c), the lower dislocation content compared with the AR material shown in Fig. 6(a) is evident from the larger spacing between dislocations. These observations are consistent with previous observations of defect structures in Zr–2.5Nb pressure tube materials subjected to different thermo-mechanical treatments [26] and with a lower dislocation density in cold-worked Zr–2.5Nb pressure tube materials heat treated at 773 K compared with those heat treated at 673 K [1,2,27].

The present observations thus show that, in the absence of irradiation, a minor improvement in corrosion response due to heat treatment in cold worked pressure tube materials may be associated with a more recovered dislocation substructure, rather than changes in the Nb content of α-Zr. The association of differences in dislocation substructure in heat-treated material with differences in corrosion behaviour implies an interaction between the lattice defects and the oxide growth front [28,29].

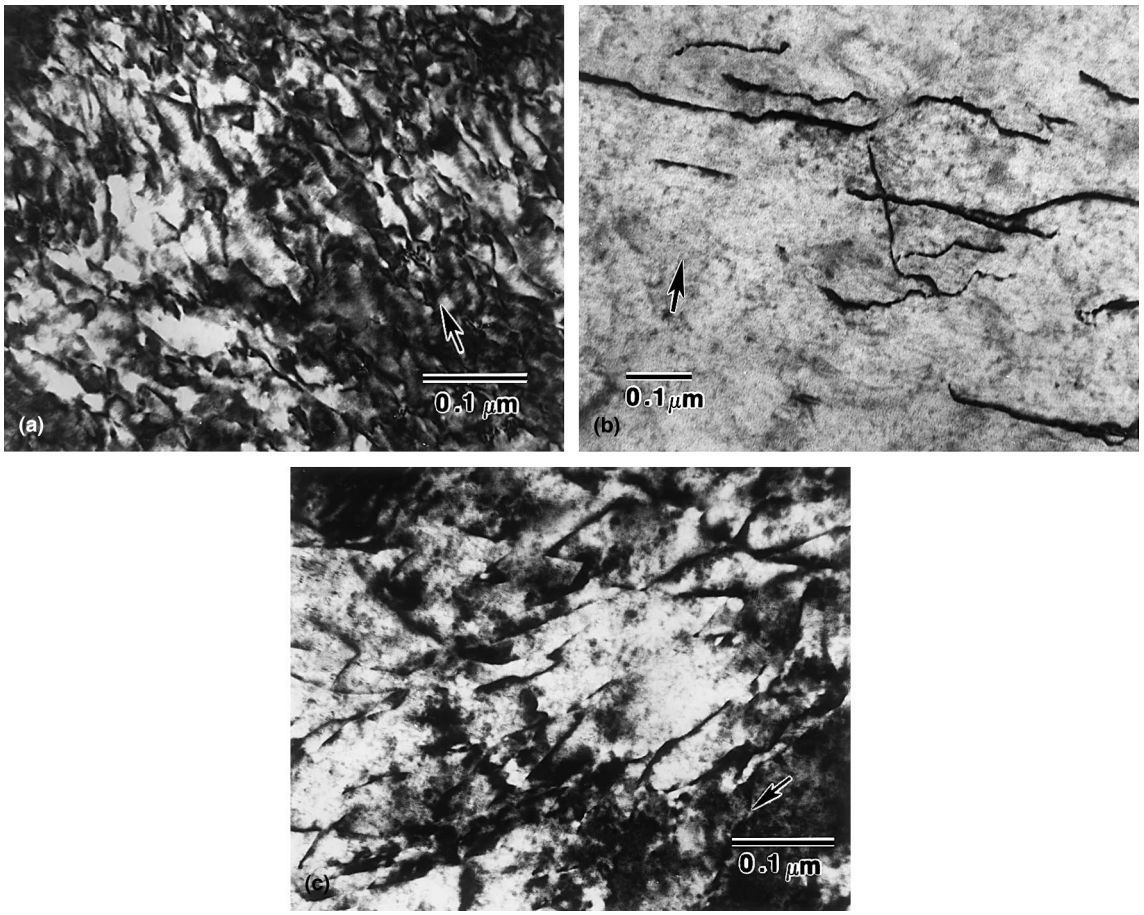

Fig. 6. TEM micrographs showing (a) a high density of ⟨a⟩-component dislocations in the AR material, (b) the presence of ⟨c⟩-component dislocations in the AR material and (c) partially recovered ⟨a⟩-component dislocations in material heat treated at 773 K for 6 h. Arrows indicate the $\mathbf{g}_{1\,0\,\bar{1}\,1}$ diffracting vector in (a) and (c) and $\mathbf{g}_{0002}$ in (b).

3.4. Variations in hydrogen pickup

Considerable variations in hydrogen pickup during a 120-day exposure to lithiated water at 583 K were found due to variations in sample surface orientations and prior heat treatments, Tables 4 and 5. Inspection of the data shows that the long prefilm period employed for some of the samples did not yield a consistent effect, even for the RN-AR material, which showed significant differences in oxide thickness. The data are therefore grouped by their type (RN, which includes the RN, RN-a and RN-b samples, or non-RN, which includes the TN, AN and AN-a samples) and prior heat treatment (AR, 673 K treated or 773 K treated). In Table 4, the hydrogen pickup data are expressed on a per unit (surface) area basis, which takes variations in coupon thickness into account. In Fig. 7, the data are plotted as a function of the oxide thickness increase during the exposure (from Table 3). The hydrogen pickup data are also expressed on a percentage basis in Table 5 and similarly plotted in Fig. 8 against the thickness increase (from Table 3). The percentage pickup represents the amount of hydrogen picked up as a percentage of the total hydrogen released due to corrosion. The percentage was derived assuming an overall oxide thickness change of twice the increase measured on one surface given in Table 3. From Figs. 7 and 8, it is clear that the variation with incremental thickness is not significant, and that it would be sufficient to compare the incremental pickup (Table 4) or its percentage (Table 5) amongst the groups. The differences between data groups for percentage hydrogen pickup, Table 5 (and Fig. 8), were investigated using the Student-t significance analysis and given in Table 6. Similar results were obtained for the pickup data in Table 4. The analysis results in Table 6 are given in terms of the probability of no difference between two groups of data; it is common practice to consider a probability of <0.05 (95% confidence level) as indicating a significant difference.

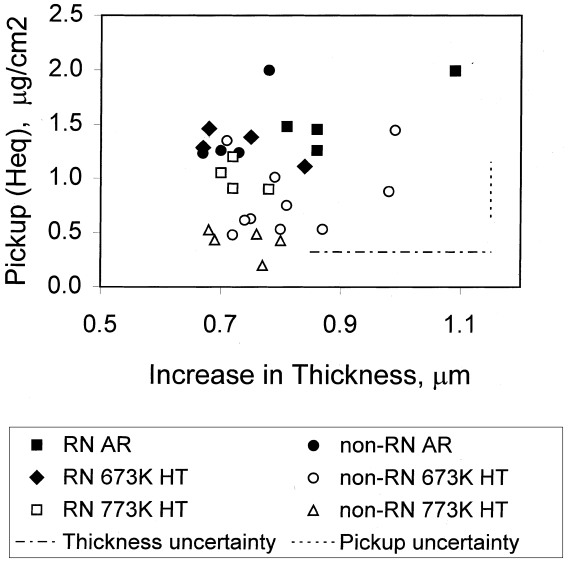

Fig. 7. Incremental hydrogen pickup per unit area versus oxide thickness change during 120-day exposure at 583 K.

Tables 4–6 and Figs. 7 and 8, show that RN and non-RN samples behaved differently with respect to hydrogen pickup. The non-RN samples showed a reduction in pickup and percentage pickup due to prior heat treatment; there being a greater reduction for the 773 K treated compared with the 673 K treated material. The RN samples showed less variation due to prior heat treatment, although the data do suggest a lower level of hydrogen pickup for the 773 K treated material, but at a lower level of significance. It is expected that longer exposures would reveal more clearly the beneficial effect due to heat treatment for the RN samples. Present results are consistent with previous reports that an improvement in corrosion behaviour due to heat treatment was accompanied by a reduction in hydrogen pickup [25].

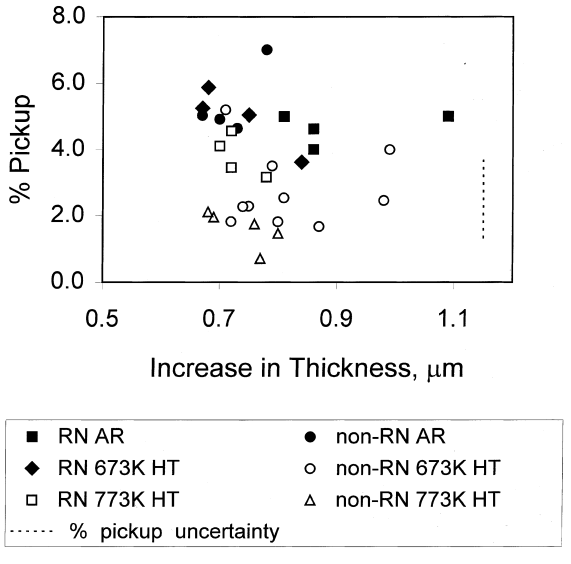

Fig. 8. Percentage hydrogen pickup versus oxide thickness change during 120-day exposure at 583 K.

The percentage hydrogen pickup data (Table 5) can be considered in relation to the oxide thickness at the beginning of the 120-day exposure (Table 2). Results for the non-RN orientations appeared to indicate that, depending on the heat treatment applied, an increase in percentage pickup could be associated with a greater oxide thickness at the beginning of the pickup measurement. However, present results also showed that all AR materials exhibited a similar percentage uptake of about 5%, while the oxide thickness varied between 1.7 and 3.0 μm depending on the surface orientation. For the heat-treated materials, the oxide thickness on different surfaces were comparable (about 1.8 μm for the 673 K treated and 1.5 μm for the 773 K treated materials), yet the percentage pickup varied between about 2% and 5% depending on the surface orientation. The percentage hydrogen pickup at a given oxide thickness is therefore not a simple function of the oxide thickness; this is another manifestation of the significance of the alloy and hence oxide microstructures.

The RN and non-RN surfaces used in the present work can be considered as extreme cases of pressure tube microstructure in terms of the β-Zr morphology. However, pressure tubes are known to contain microstructural inhomogeneities. There may be local regions in the RN surface where more β-Zr filaments are aligned perpendicular to the surface. The range of percentage hydrogen pickup observed in the present work is consistent with the 3–7% range typically observed for Zr–2.5Nb [25,30]. Present results indicate that the differences in the β-Zr morphology and the extent of decomposition could provide a basis for rationalising, at least in part, the variations in percentage pickup between different Zr–2.5Nb pressure tubes, or between different locations within a tube.

Since hydrogen pickup involves processes within the oxide, the microstructure of the oxide converted from β-Zr or its (partially) decomposed products becomes important. Some characteristics of corrosion products from the single phase β-Zr (Zr–20Nb) alloy and from β-Zr and β-Nb in Zr–2.5Nb pressure tubes have been reported recently [31,32]. The characteristics of oxidised β-regions were found to be related to the β-phase prior to oxidation [32]. For β-Nb initially present in the alloy, two types of Nb-enriched regions in the oxide have been observed due to corrosion exposures, a microcrystalline sub-oxide based on β-Nb was observed close to the interface, while amorphous oxidised β-Nb was observed due to more complete oxidation further away from the

Table 6
Probability for no difference between groups. The mean and standard deviation for percentage pickup in each group are given in brackets

	RN-673 K (4.69/0.64)	RN-773 K (3.98/0.73)	Non-RN AR (5.50/1.06)	Non-RN 673 K (2.78/1.13)	Non-RN 773 K (1.60/0.30)	Non-RN 673 K + 773 K (2.38/1.11)
RN-AR (4.55/0.51)	0.371	0.123	0.077	–	–	–
RN-673 K (4.69/0.64)	–	0.096	–	4.3×10^{-3}	–	–
RN-773 K (3.98/0.73)	–	–	–	–	4.0×10^{-4}	–
RN-all (4.40/0.66)	–	–	–	–	–	4.6×10^{-6}
Non-RN AR (5.50/1.06)	–	–	–	6.9×10^{-4}	8.8×10^{-5}	5.2×10^{-5}
Non-RN 673 K (2.78/1.13)	–	–	–	–	0.025	–

interface [32]. An example of a microcrystalline Nb-rich region in an oxide thin foil immediately adjacent to the metal interface is shown in Fig. 9, for a 773 K heat-treated material prefilmed for 24 h at 673 K and exposed to a total of 176 days in lithiated water at 583 K.

Present results suggest that both the nature of Nb-enriched regions in the oxide and the connectivity of these regions affected hydrogen pickup. In addition, the relatively high level of pickup for the RN samples may be significant and suggests the possible presence of another hydrogen pickup process not related to β-Zr. One possibility is that the diffusional characteristics of the RN oxides are different than those of the non-RN oxides, on account of the different oxide microstructure and microtextures arising from differences in the metal surface orientation [33–35].

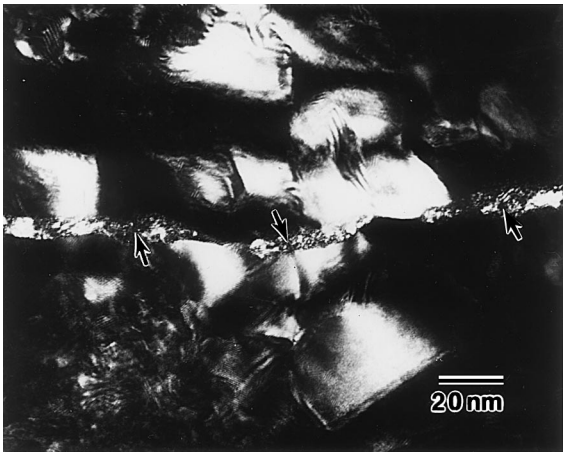

Fig. 9. Dark field, plan-view TEM micrograph of microcrystalline Nb-enriched region (arrowed) formed from β-Nb in oxide immediately adjacent to the interface with metal; sample was heat treated at 773 K, prefilmed at 673 K for 24 h and exposed to lithiated water at 583 K for a total of 176 days.

4. Conclusions

In the absence of a significant variation in the alloy composition or impurity content, the corrosion and hydrogen pickup of Zr–2.5Nb pressure tube materials can be influenced by the morphology of β-Zr and by heat treatments which affected primarily the decomposition of β-Zr. The influences are different with respect to corrosion and hydrogen pickup, i.e. the variability in corrosion and hydrogen pickup are due to different causes.

An enhanced overall oxide growth is identified with β-Zr initially in the undecomposed state and aligned primarily perpendicular to oxide surface. Decomposing the β-Zr prior to corrosion exposures eliminated this enhanced growth. A minor improvement in corrosion resistance due to heat treatment is attributed to the recovery of lattice defects in α-Zr, rather than changes in the Nb content in α-Zr, which did not vary significantly with heat treatment or exposure.

A significant reduction in hydrogen pickup due to prior heat treatment can be associated with the decomposition of β-Zr when the β-Zr was aligned primarily perpendicular to the oxide surface and less significant when the β-Zr was primarily parallel with the oxide surface. The instantaneous percentage hydrogen pickup at a given oxide thickness is not a simple function of the oxide thickness.

Acknowledgements

This work was supported by funding from Ontario Hydro. Helpful discussions with M. Leger are gratefully acknowledged. The technical assistance of R. Jarochowicz is also acknowledged.

References

[1] R.G. Fleck, E.G. Price, B.A. Cheadle, ASTM STP 824 (1984) 88.
[2] M. Leger, R.G. Fleck, ASTM STP 824 (1984) 409.

[3] B.A. Cheadle, S. Aldridge, J. Nucl. Mater. 47 (1973) 255.
[4] V.F. Urbanic, B.D. Warr, A. Manolescu, C.K. Chow, M.W. Shanahan, ASTM STP 1023 (1989) 20.
[5] B.D. Warr, Ontario Hydro, Toronto, unpublished results.
[6] V.F. Urbanic, P.K. Chan, D. Khatamian, O.T. Woo, ASTM STP 1245 (1994) 116.
[7] V.F. Urbanic, R.W. Gilbert, Proceedings of the Technical Committee Meeting on Fundamental Aspects of Corrosion on Zirconium Base Alloys in Water Reactor Environments, Portland, Oregon, USA, 11–15 September 1989, IAEA, Vienna, 1990, p. 262.
[8] V.F. Urbanic, R. Choubey, C.K. Chow, ASTM STP 1132 (1991) 665.
[9] B.D. Warr, E. Rasile, A.M. Brennenstuhl, Proceedings of the Technical Committee Meeting on Fundamental Aspects of Corrosion on Zirconium Base Alloys in Water Reactor Environments, Portland, Oregon, USA, 11–15 September 1989, IAEA, Vienna, 1990, p. 124.
[10] Y. Ding, D.O. Northwood, J. Mater. Sci. 27 (1992) 1045.
[11] A. Perovic, V. Perovic, G.C. Weatherley, G.R. Purdy, R.G. Fleck, J. Nucl. Mater. 199 (1993) 102.
[12] V. Perovic, A. Perovic, G.C. Weatherley, L.M. Brown, G.R. Purdy, R.G. Fleck, R.A. Holt, J. Nucl. Mater. 205 (1993) 251.
[13] K.N. Choo, Y.H. Kang, S.I. Pyun, V.F. Urbanic, J. Nucl. Mater. 209 (1994) 226.
[14] C.E. Lundin, R.H. Cox, USAEC Report GEAP-4089, (1962) 9.
[15] A. Fernandez Guillermet, Z. Metallkund. 82 (1991) 478.
[16] D.G. Lees, Coros. Sci. 5 (1965) 565.
[17] J.E. LeSurf, ASTM STP 458 (1969) 286.
[18] V.F. Urbanic, J.E. LeSurf, A.B. Johnson, Corrosion 31 (1975) 15.
[19] B. Cox, Long-Term Oxidation of Zr-2.5 wt% Nb Alloy, Atomic Energy Canada Limited, AECL-5610, 1976.
[20] L.V. Ramanathan, I. Costa, W.A. Monteiro, J. Testing Evaluation 17 (1989) 172.
[21] A.J.G. Maroto, R. Bordoni, M. Villegas, A.M. Olmedo, M.A. Blesa, A. Iglesias, P. Koenig, J. Nucl. Mater. 229 (1996) 79.
[22] S.B. Dalgaard, The Corrosion Resistance of Zr–Nb and Zr–Nb–Sn Alloys in High-Temperature Water and Steam-Part II, Atomic Energy Canada Limited, AECL-1308, 1961.
[23] I.A. El-Shanshoury, V.A. Rudenko, M.E. El-Dahshan, Corros. Sci. 9 (1969) 479.
[24] B. Cox, In: M.G. Fontana, R.W. Staehle (Eds.), Advances in Corrosion Science and Technology, vol. 5, Plenum, New York, 1976, p. 173.
[25] V.F. Urbanic, M. Griffiths, Proceedings of the 12th International Symposium: Zirconium in the Nuclear Industry, Toronto, Ontario, Canada, 15–18 June 1998, ASTM-STP, 1354 Philadelphia.
[26] V. Perovic, G.C. Weatherley, R.G. Fleck, Can. Metall. Quart. 24 (1985) 253.
[27] R.A. Holt, J. Nucl. Mater. 59 (1976) 234.
[28] H.E. Evans, D.J. Norfolk, T. Swan, J. Electrochem. Soc. 125 (1978) 1180.
[29] H.E. Evans, Int. Mater. Rev. 40 (1995) 1.
[30] N. Ramasubramanian, V. Perovic, M. Leger, Proceedings of the 12th International Symposium: Zirconium in the Nuclear Industry, Toronto, Ontario, Canada, 15–18 June 1998, ASTM-STP 1354, Philadelphia.
[31] O.T. Woo, Y.P. Lin, J. Nucl. Mater., accepted for publication.
[32] Y.P. Lin, In: S.B. Newcomb, J.A. Little (Eds.), Microscopy of Oxidation 3, The Institute of Materials, London, 1997, p. 462.
[33] Y.P. Lin, O.T. Woo, D.J. Lockwood, Mater. Res. Soc. Symp. Proc. 343 (1994) 487.
[34] M.G. Glavicic, J.A. Szpunar, Y.P. Lin, J. Nucl. Mater. 245 (1997) 147.
[35] V.Y. Gertsman, Y.P. Lin, A.P. Zhilyaev, J.A. Szpunar, Philos. Mag., accepted for publication.